Enhancement of Structural Fluctuation in the Region Connecting Two Kinds of Critical Points in Temperature−Pressure−Composition Three-Dimensional Phase Diagram: Raman Studies of Benzene/CO_2 Binary Systems up to Supercritical Region

Hideyuki Nakayama, Miki Murai, Mariko Tono-oka, Kumiko Masuda, and Kikujiro Ishii*

Department of Chemistry, Gakushuin University, 1-5-1 Mejiro, Toshimaku, Tokyo, 171-8588 Japan

Received: August 9, 2006; In Final Form: December 25, 2006

Pressure dependence of Raman spectra of benzene/CO_2 two-component systems was systematically studied at different temperatures and compositions. We estimated the magnitude of inhomogeneous component in Raman bandwidth to get information on the structural fluctuation in the system. It was found that the inhomogeneous bandwidth attains a maximum on an isothermal plane in the temperature−pressure−composition three-dimensional phase diagram when the state point crosses the line connecting the region where the density fluctuation is large (the vicinity of the critical point of neat CO_2) and the region where the concentration fluctuation in a binary system is enhanced (the vicinity of the critical solution point). By accumulating such data, we found that the points of large structural fluctuation comprise a sheet that includes the extension line of the gas−liquid equilibrium line in the phase diagram of neat CO_2 and the line connecting critical solution points of the two-component system at different temperatures. Interaction between benzene and CO_2 molecules in the supercritical region is briefly discussed.

1. Introduction

Supercritical fluids have attracted widespread attention in the last several decades as useful solvents, owing to their versatile properties that can be continuously controlled by changing their density.[1,2] Furthermore, supercritical water and CO_2 are anticipated to be green solvents that do not trouble nature when we put them back into the environment. From the standpoint of basic chemistry, however, it is still important to study the structure and dynamics of supercritical fluids, and active studies are thus performed currently by various experimental and theoretical methods.[3] Fluctuation is an important concept in these studies.[4] There arise two kinds of fluctuations in solutions: density fluctuation (DF) and concentration fluctuation (CF). We use in this paper the term structural fluctuation (SF) when we refer to both of them.

DF in a neat compound is enhanced in the vicinity of the critical point, and the divergent behaviors have been elucidated in the earlier stage of the study of supercritical fluids.[5] Recently, Nishikawa and co-workers[6,7] studied small-angle X-ray scattering on a number of compounds in supercritical states and experimentally showed that the region of large DF extends in general in the temperature−pressure phase diagram along a line that is the extension of the gas−liquid equilibrium line. We call this extension line the "ridge" of DF according to Nishikawa and co-workers. They pointed out that the concept of DF is important in understanding the nature of supercritical fluids, since various physicochemical quantities such as partial molar volume, solubility, and reactivity show anomalies on this ridge. We also demonstrated that this ridge qualitatively divides the supercritical region into the gas-like and liquid-like regions by showing the distribution of Raman bandwidth of the molecule.[8]

When we regard supercritical fluids as solvents, it is naturally important to understand CF. CF occurs even in ideal solutions, but it is known to appear in an enhanced manner in some special situations. The examples are the critical CF[5] and the CF due to solvation.[9] Critical CF arises in systems that have a critical point of mutual miscibility. Few cases of it have been studied for supercritical states. Scheerboon and Schouten[10] reported the Raman studies of it for He/N_2 systems. CF due to solvation is said in other words to be the inhomogeneous solution structure resulting from the attractive interaction between the solute and solvent molecules[3,11] and is important in cluster formation in supercritical solutions. Many studies have been made on this type of CF[3,4] from the viewpoints of density dependence of the solvation-region size or local enhancement of density. However, few such studies on supercritical solutions have been made by making the sample state clear in the phase diagram of the system.

Ikawa and co-workers[12,13] measured the infrared and near-infrared spectra of water/benzene systems by systematically taking the state points in the supercritical region. They found that the excess volume on mixing is enlarged in a particular region in the phase diagram. The previously mentioned X-ray studies by Nishikawa and co-workers[6,7] and our Raman studies[8] were those in which they were strongly conscious of the thermodynamic state of the sample, although the systems studied there were single-component. Such studies have given new viewpoints to this field of physical chemistry. In extending our study to two-component systems, we have then systematically studied the distribution of SF in the temperature−pressure−composition (TPC) three-dimensional phase diagram.

Phase equilibrium is the crucial issue in the application of supercritical fluids. Great efforts thus have been made on it.[14,15] In the present study, we choose the benzene/CO_2 binary system, since its phase diagram have been studied in TPC space including the critical points.[16,17] We reproduce the data for benzene/CO_2 in Figure 1. Such phase diagrams have a characteristic upper critical solution point in the pressure−concentra-

* To whom correspondence should be addressed: e-mail kiku.ishii@gakushuin.ac.jp.

10.1021/jp0651485 CCC: $37.00
Published on Web 02/06/2007

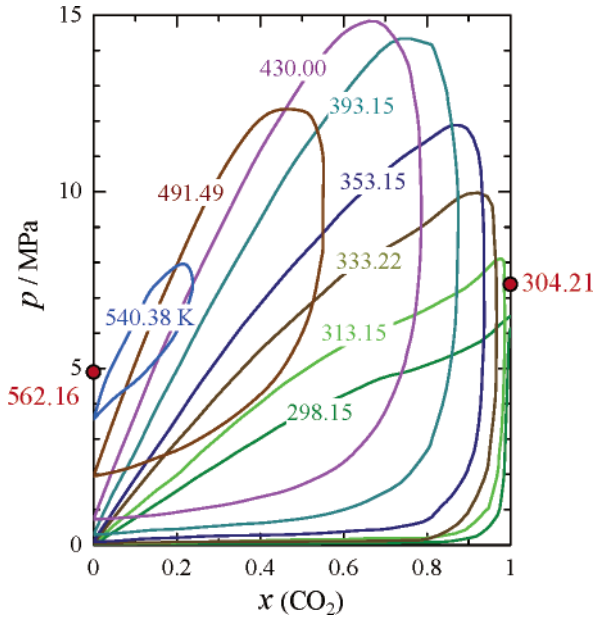

Figure 1. Phase-separation curves of the benzene/CO_2 binary system at different temperatures indicated in kelvins. Abscissa represents the mole fraction of CO_2, and ordinate represents the total pressure (reproduced from the data in refs 16 and 17). The critical pressures of pure benzene and pure CO_2 are plotted with red circles, and the critical temperatures are noted beside the plots.

tion (PC) two-dimensional phase diagram in an isothermal plane, which is classified into one of the most typical diagrams for two-component systems related to gaseous and liquid states.[18] The state regions with which we were concerned in the present work were the vicinity of the critical point of the neat CO_2 and that of the critical solution points of the benzene/CO_2 system. We anticipated that different kinds of fluctuations occur in these regions.

We employed Raman scattering to study SF in supercritical solutions. We have already shown that Raman bandwidths are strongly related to DF of supercritical fluids.[8,19] Similar studies have been made in relation to CF of two-component solutions under atmospheric pressure.[20] It should be noted, however, that we cannot simply estimate the magnitude of the inhomogeneity component from the total Raman bandwidth that is in general the superposition of the width arising from the sample inhomogeneity and the width arising from a finite lifetime of the excited state of the molecule. In addition, we cannot simply separate the contributions coming from DF and CF causing the inhomogeneous width. We therefore had to make analyses of Raman bandwidths in this study on several ad hoc assumptions. However, the results obtained are reasonable in light of physicochemical intuition and bring us new viewpoints on the characteristics of supercritical fluids as solvents.

2. Experiments and Data Analyses

The schematic diagram of the high-pressure sampling system and the cross section of the high-pressure Raman cell are shown in Figures 2 and 3. Liquid CO_2 and benzene were pressurized by use of SCF-GET and PD-1580 pumps (Jasco), respectively, and mixed in a 2 m long stainless tube that supplied the solution into the cell. In the middle of the above tube, a membrane filter with 0.1 μm pores (Toyo Roshi, Ltd.) was inserted to remove dust. The sample pressure was controlled by use of an automated exhaust valve (SCF-Bpg, Jasco) that was attached to the outlet of the cell. The pressure was monitored with a strain gauge (RH-300KB, Kyowa Dengyo Co.).

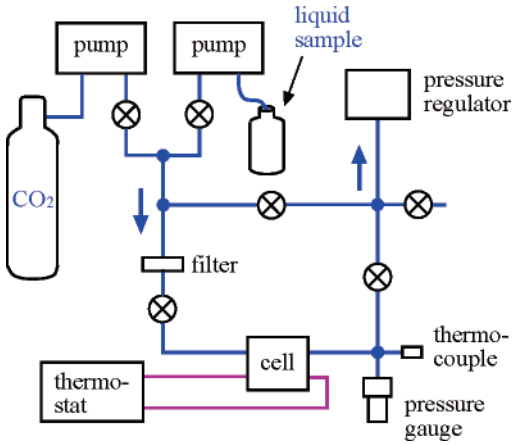

Figure 2. High-pressure sampling system for Raman measurements on supercritical binary solutions. The cell temperature was controlled by circulation of warmed water and a thermostat. The sample pressure was changed by releasing the sample from the cell stepwise through the pressure regulator.

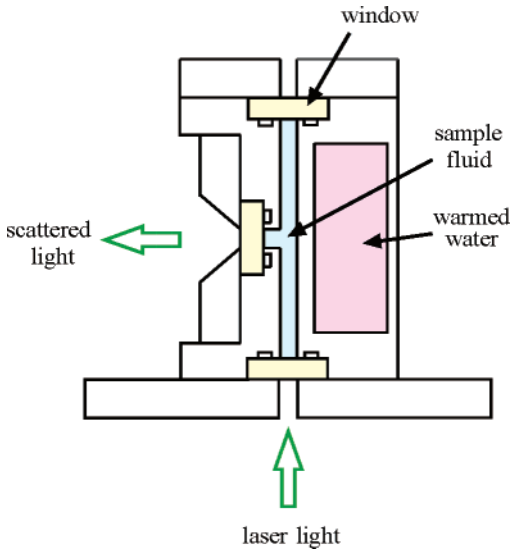

Figure 3. Cross section of the high-pressure Raman cell. The inlet and outlet ports for the sample were equipped in the direction perpendicular to this cross section. Warmed water was circulated through the cave made in the stainless-steel block.

The Raman cell was made with stainless steel and was equipped with three optical ports of 7-mm-thick glass. O-rings made of synthesized rubber (Kalrez, DuPont Co.) were used as the gaskets. A cave was made in the stainless-steel block of the cell to control the sample temperature by circulating warmed water through it. A thermostat (DC30-K20, Haake) was used for this, and the sample temperature was monitored with a chromel−alumel thermocouple inserted into the sample fluid near the position where Raman scattering was measured. We carefully adjusted the temperature of the thermostat, since the thermal properties of the sample were different at different pressures and the DF and/or CF in the vicinities of the critical points caused a slight thermal effect of the laser-light scattering. The fluctuations of the temperature and pressure during the Raman measurement at a particular set of conditions were ±0.1 K and ±0.01 MPa, respectively.

Raman measurements were performed on a single monochromator (Triax-550, Jobin Yvon-Spex) equipped with a charge-coupled device (CCD) photodetector (Spectrum-One, Jobin Yvon-Spex). An Ar^+-ion laser (GLG-3260, NEC Co.) operated at 514.5 nm was used for the Raman excitation, with

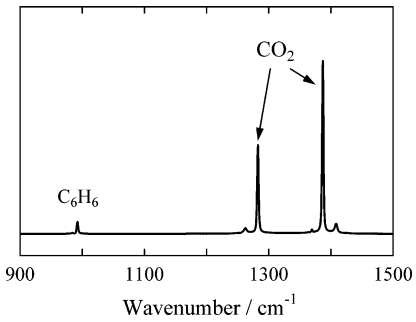

Figure 4. Raman spectrum of a benzene/CO_2 system at 322.5 K and 17.5 MPa. The mole fraction of CO_2 was 0.994. Three small bands near the strong bands of CO_2 around 1280 and 1380 cm^{-1} (the Fermi dyad) are attributed to CO_2 molecules with heavy isotopes.

power of 100 mW at the laser incidence port of the cell. The scattered Raman light was collected at 90° with ss polarization. The laser beam diameter at the measuring region was estimated to be about 0.04 mm from the focal length of the collimator lens and the beam size of the laser. This measuring region made its image of a 0.06 mm width and of a sufficient length on the monochromator slit of a 0.05 mm width through the glass window of the cell and the lenses for the collection of the Raman light. For the reduction of the elastically scattered light, a notch filter (Super-notch, Kaiser Optical Systems) was used. The spectral slit width of the monochromator was 1.5 cm^{-1}.

Liquid CO_2 (99.99%, Showa Tansan Co.) was used without further treatment. Benzene (Wako Pure Chemical) was used after distillation of the reagent-grade liquid that was dehydrated in advance with molecular sieves. Preparation of the sample fluid at a particular condition was as follows. First, liquid CO_2 and benzene were pressurized into the Raman cell with certain flow rates at the maximum pressure desired. During this process, Raman band intensities of both compounds were monitored, and the flow rate of each compound was adjusted so as to attain the desired sample composition. When the desired composition was approximately established, the valves at the inlet and outlet of the cell were closed, and Raman measurements at the maximum pressure were performed. We confirmed at this stage that the observed spectral features did not change at least for 30 min. After this, we released stepwise a portion of the sample outside the cell by monitoring the pressure gauge, and we repeated the Raman measurements at different pressures.

We determined the sample composition at every pressure using the intensity ratio of the Raman bands of benzene around 992 cm^{-1} and of CO_2 around 1283 cm^{-1} (see Figure 4). This ratio was studied in advance by use of benzene solutions in room-temperature CO_2 liquid of known compositions. In this experiment, high-pressure glass tubes (HPG-10, Taiatsu Techno Co.) were used as the Raman cell. The amount of benzene was measured by weighing, and that of CO_2 was estimated before the condensation from the gas pressure in a vessel with a known volume. The wavenumber, width, and intensity of each Raman band were analyzed by fitting with Lorentz-type functions. We examined also Gauss-type functions, but better results were obtained by use of the former functions in a wide range of pressure. We thus analyzed the properties of the observed Raman bands by fitting with Lorentz-type functions throughout this work to avoid discontinuity in the series of the data obtained by changing the temperature, pressure, and composition of the sample. The band intensity referred to in this paper is the integrated intensity.

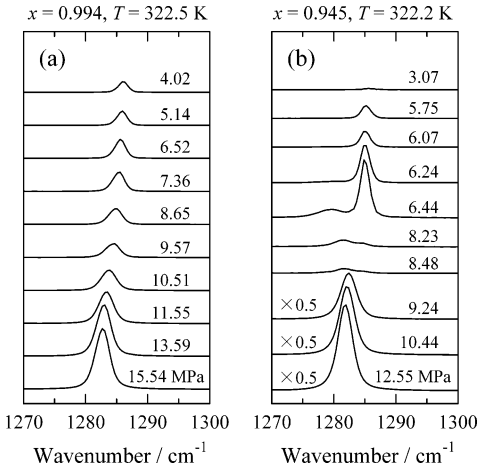

Figure 5. Evolution of one band of the Fermi dyad of CO_2 observed for two samples by decreasing the pressure.

3. Results and Discussion

3.1. Examples of Observed Raman Spectra and the State of the Sample. An example of the Raman spectrum of benzene/CO_2 binary systems is shown in Figure 4. It was measured at 322.5 K and 17.5 MPa, and the mole fraction $x(CO_2)$ was 0.994. The bands at 1283 and 1388 cm^{-1} of CO_2 (so-called Fermi dyad) are those brought about by the Fermi resonance between the symmetric C═O stretching mode and the overtone of the O−C−O bending mode. The weak 992 cm^{-1} band is attributed to the breathing mode of benzene. We used this band in the present study as the band that represents the molecular state of benzene, since this is the strongest among the benzene Raman bands.

Figure 5 shows the evolution of one band of the CO_2 Fermi dyad observed by decreasing the pressure. Spectra shown in Figure 5a were obtained for the sample with $x(CO_2)$ 0.994 at the start of the experiment at 322.5 K and 15.54 MPa. Spectra shown in Figure 5b were obtained for the sample with $x(CO_2)$ 0.945 at the start of the experiment at 322.2 K and 12.55 MPa. Sample temperature during a series of measurements for a particular sample was kept at the temperature indicated above, while small changes in the mole fraction took place as the pressure was reduced stepwise. The latter problem will be mentioned later in detail at the end of this section.

For the sample of Figure 5a, the Raman intensity decreased in the vicinity of 9 MPa. This is due to the density decrease in this pressure region, and also due to the enhanced scattering of the excitation laser light[21] when the sample state passed in the phase diagram the region near the critical point of neat CO_2. The latter cause included two features. First, the intensity of the laser light at the measuring position in the sample was diminished by the light scattering in the incident path. For the second, the efficiency of the Raman light collection at the monochromator slit decreased, owing to the hazed image of the measuring region due to the light scattering. However, such degradation in the optical condition is not considered to have modified the Raman bandwidth in the present study. This is because the change in direction of the Raman scattering vector might have brought about the appearance of a weak component of sp polarization, but we were measuring the much stronger component of ss polarization.

For the sample of Figure 5b, the Raman intensity decreased significantly in the vicinity of 9 MPa, and in addition, the band split into two at lower pressures. The decrease in intensity is attributed to the laser-light scattering due to the concentration

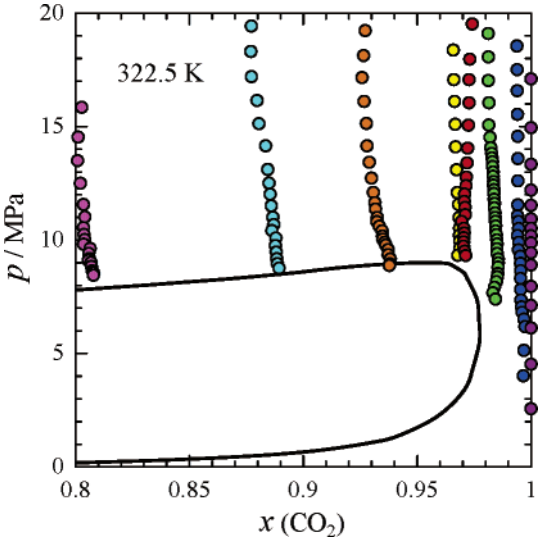

Figure 6. Change of the composition of different binary samples due to the stepwise lowering of the pressure at 322.5 K. The solid curve represents the phase-separation curve at this temperature obtained by interpolation of the data in Figure 1.

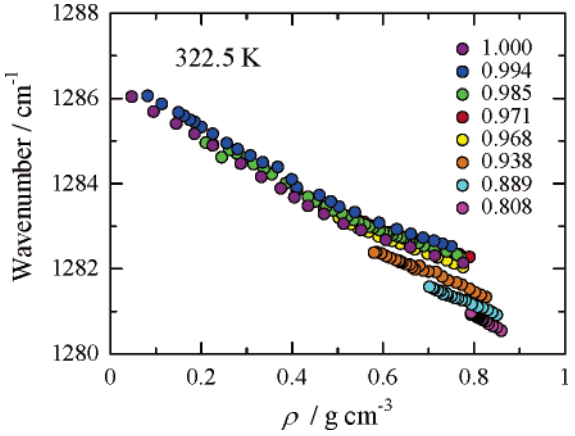

Figure 7. Density dependence of the wavenumber of one band of the Fermi dyad of CO_2 observed for samples with different CO_2 mole fractions at 322.5 K. The mole fractions of CO_2 of the samples distinguished by the colors are indicated with the values at which enhanced structural fluctuations were observed (section 3.1).

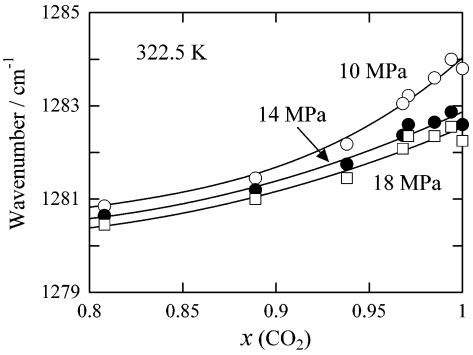

Figure 8. Composition dependence of the wavenumber of the CO_2 band estimated for three constant pressures. The original data were the same as those used to depict Figure 7.

fluctuations in the vicinity of the critical solution point, while the splitting at lower pressures is attributed to the separation of solution into two phases. In fact, we saw a phase boundary between these phases through the optical port of the Raman cell. We confirmed that the band of the smaller wavenumber came from the phase with the larger density (at the bottom in the cell) and the band of the larger wavenumber came from the phase with the smaller density (at the top in the cell) by separately recording the scattered lights by use of a cover plate in front of the slit of the spectrometer. It is considered from the shapes of the phase-separation curves in Figure 1 that the bottom phase was the benzene-rich phase and the top phase was the CO_2-rich phase. The intensity ratio between the split bands reflects the volumes of the two phases actually observed from the direction of the spectrometer. When the sample pressure was reduced further, the band at the smaller wavenumber disappeared, since the level of the phase boundary was lowered below the bottom of the observation port of the cell.

Before proceeding to discuss the detailed analyses of Raman spectra, an issue related to the composition of each sample warrants explanation. Figure 6 shows the change of composition of benzene/CO_2 samples measured while lowering the pressure stepwise at 322.5 K. The composition of each sample changed a little as a portion of the sample was released outside stepwise to lower the pressure. This is considered due to the inhomogeneous distribution of the sample composition throughout the high-pressure system including the tubing. In the later discussion on the enhancement of fluctuations in the vicinity of the critical points, we will refer to each sample using the composition at the pressure relevant to the fluctuation enhancement.

3.2. Density and Composition Dependences of Raman-Band Wavenumber. For a Raman bandwidth to reflect the magnitude of DF and CF, the corresponding vibrational wavenumber ν of the molecule must depend on the density and composition, respectively. Thus we examined the behaviors of benzene and CO_2 bands by changing these parameters.

Figure 7 shows the density dependence of the wavenumber of the CO_2 Raman band around 1280 cm^{-1} for samples with different compositions. The method of the density estimation will be described later in section 3.4 and in the Appendix. The composition dependence of the wavenumber of the same Raman band is, on the other hand, shown in Figure 8 for different pressures. The data plotted in this figure were obtained by extrapolating or interpolating the data at different pressures to the pressures indicated in the figure. As the density increases or as the benzene content increases, the CO_2 band shifts to the small-wavenumber side. This implies that the corresponding vibrational mode that involves the changes in the dipole and quadrupole moments is stabilized by the electronic polarization of the surrounding molecules. We examined another Raman band of CO_2 around 1380 cm^{-1} as well as the benzene band around 990 cm^{-1}, but we could not find bands whose wavenumbers were more sensitive to density or composition. Thus we studied the structural fluctuations in benzene/CO_2 systems by focusing on the CO_2 band around 1280 cm^{-1}. In the remaining part of this paper, we discuss the band wavenumber or width without mentioning that we are discussing the behavior of this band. Thus the fluctuations discussed in this paper are those seen through the behavior of this molecular vibration of CO_2.

3.3. Pressure Dependence of Bandwidth. We measured pressure dependence of Raman spectra of benzene/CO_2 systems as a function of composition at 313.2, 322.5, and 333.2 K. The data points already shown in Figure 6 were the records of the actual composition of the samples during such experiments at 322.5 K. The solid curve in this figure represents the equilibrium compositions of the two phases as a function of pressure at this temperature.[16] The samples with $x(CO_2)$ larger than 0.98 at the

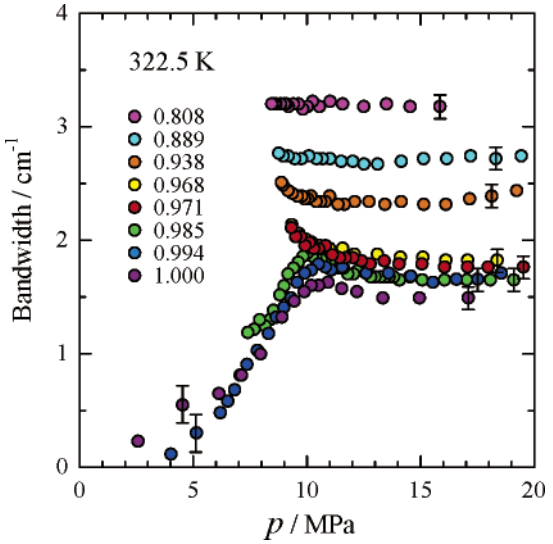

Figure 9. Pressure dependence of the bandwidth of the same CO_2 band as in Figures 7 and 8 observed for different samples at 322.5 K. The CO_2 mole fractions of the samples distinguished by the colors are indicated. The error bars attached to several data points represent the estimated possible error in the bandwidth correction for the spectral slit width (see text). The error bars drawn in other figures correspond to these error bars in this figure.

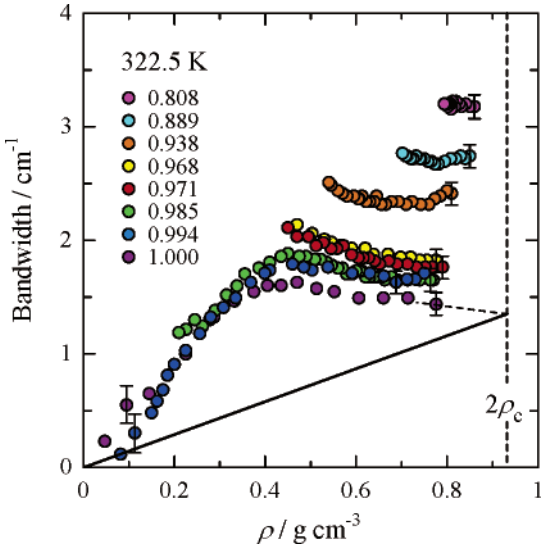

Figure 10. Bandwidth of the same CO_2 band as in Figures 7−9 observed for different samples at 322.5 K. The data are the same as those in Figure 9, but the abscissa has been transformed from pressure to density. (---) Density twice the ρ_c of neat CO_2; (—) density-dependent contribution of the homogeneous broadening of neat CO_2.

start of the experiments did not undergo phase separation until the lowest pressure, but the samples with smaller $x(CO_2)$ showed phase separation in the vicinity of 9 MPa. For these samples, the data point of the lowest pressure (the final datum plotted in this figure) represents the composition of the single-phase state measured just before the phase separation.

Figure 9 shows the pressure dependence of the bandwidth at 322.5 K of the same samples as for Figures 6 and 7. The bandwidths discussed hereafter were corrected for the spectral slit width of the monochromator, 1.5 cm^{-1}, by the method of Tanabe and Hiraishi.[22] The error in the corrected width obtained by this method was estimated as small as 0.2 cm^{-1} even for a band of apparent width as small as 2 cm^{-1}. We indicated the magnitude of possible error in the estimation of bandwidth with error bars in Figure 9. The three samples of $x(CO_2) = 1.000$, 0.994, and 0.985 did not undergo phase separation. Their bandwidth showed a slight increase first, as the pressure was lowered, and then decreased in the low-pressure region after passing a peak around 10 MPa. The awkward changes recorded in the lowest pressure region are due to the smallness of the original bandwidth. For the samples with $x(CO_2)$ smaller than 0.98, the data plotting stops at certain pressures because of the phase separation. Among these, the samples with $x(CO_2) = 0.971$, 0.968, and 0.938 showed a remarkable increase in the bandwidth as the pressure approached the point of phase separation. However, the samples with $x(CO_2) = 0.889$ and 0.808 did not show such an increase although the magnitude of the bandwidth itself was larger. Results similar to those shown in Figure 9 were obtained at 313.2 and 333.2 K.

3.4. Estimation of Inhomogeneous Bandwidth. For relating the observed bandwidth to the microscopic structure of the sample, density is a more appropriate variable than pressure, since intermolecular distances are the crucial parameter for intermolecular interactions. We therefore transformed the pressure-dependent data into density-dependent data. For this, we estimated the volume of the sample at every pressure by using the following Peng−Robinson equation that is a van der Waals-type state equation modified for the system with multiple components:[17,23]

$$p = \frac{RT}{V_{mix} - b_{mix}} - \frac{a_{mix}}{V_{mix}(V_{mix} + b_{mix}) + b_{mix}(V_{mix} - b_{mix})} \quad (1)$$

where p, T, and R are the pressure, temperature, and gas constant, respectively. The average molar volume of the mixture, V_{mix}, is equal to $V/\sum n_i$, that is, the actual volume divided by the nominal sum of the amount n_i of the ith component. The parameters a_{mix} and b_{mix} are related to the mole fraction x_i of the ith component,[17] described in detail in the Appendix. The density ρ was derived by the relationship

$$\rho = M_{mix}/V_{mix} \quad (2)$$

where $M_{mix} = \sum x_i M_i$ and M_i is the molar mass of the ith component.

Figure 10 shows the density dependence of the bandwidth transformed from the data displayed in Figure 9. The sample density was estimated by the method described above. Raman bandwidth of a condensed matter comprises in general the homogeneous and inhomogeneous components. To extract the inhomogeneous component, we thus need to estimate the magnitude of the homogeneous component.

The homogeneous bandwidth of a molecular vibration is caused by the energy and phase relaxations of the vibration, and also by the relaxation due to the orientation change of the molecule. We neglected in this work the contribution of the orientation relaxation, since we adopted the ss polarization condition in the Raman measurements and the depolarized sp spectra were very weak compared with the ss spectra. In addition, the energy relaxation time in molecular liquids is longer than the phase relaxation time, and therefore the contribution of the former relaxation to the bandwidth is smaller than that of the latter relaxation.[24] In fact, Saitow et al.[19] explained well the density dependence of the Raman bandwidth of supercritical CHF_3 by assuming only the contributions of phase relaxation and inhomogeneity. According to their estimation, the homo-

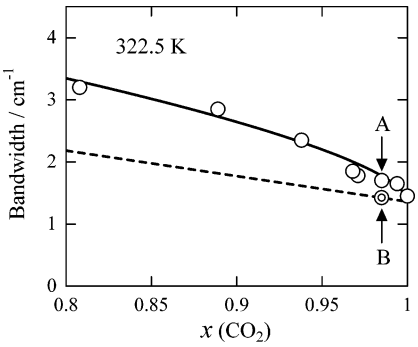

Figure 11. Estimation of homogeneous band broadening due to the addition of benzene. The plotted data indicate the bandwidth estimated by the extrapolation of the observed data at 322.5 K to $2\rho_c$. (—) Fit of the plotted data with eq 3; (---) portion of homogeneous broadening (second and third terms in eq 3) for different CO_2 mole fractions.

geneous bandwidth caused by the phase relaxation increases monotonously with density, showing a slight upward curvature, while the inhomogeneous bandwidth shows a peak around $\rho = 0.8\rho_c$ and is almost negligible at $\rho = 2\rho_c$, where ρ_c indicates the critical density of the compound. The latter estimation corresponds to the fact that DF is negligible at $\rho = 2\rho_c$ compared with the value at the peak.[25]

Taking account of the above-mentioned knowledge for the bandwidth, we will assume in the following analysis that the homogeneous bandwidth depends linearly on density (assumption 1) and that the inhomogeneous broadening due to DF diminishes at $\rho = 2\rho_c$ (assumption 2). According to these assumptions, we can draw a solid linear line in Figure 10 for the density-dependent contribution of the homogeneous broadening by extrapolating the data for neat CO_2. However, we cannot make such a simple estimation of the homogeneous contribution for binary samples, since there is still a contribution from CF to the inhomogeneous broadening even at $\rho = 2\rho_c$. We therefore took the following additional processes for estimating the contribution from CF at $\rho = 2\rho_c$.

We first extrapolated the density dependence of the bandwidth of each sample in Figure 10 to the point of $2\rho_c$. The estimated bandwidths at $2\rho_c$ for samples of CO_2-rich compositions were then assumed to be expressed by eq 3 (assumption 3):

$$\Delta\nu_{2\rho_c} = f\{x(1-x)\}^{0.5} + g(1-x) + h \qquad (3)$$

where x stands for the CO_2 mole fraction of each sample. The first term on the right-hand side of eq 3 expresses the contribution of CF within the framework of the ideal solution.[20] The second term expresses the acceleration of relaxation by the addition of benzene that possesses a larger number of vibrational modes than CO_2. The third term expresses the homogeneous width inherent in neat CO_2. We plotted the extrapolated widths for different samples in Figure 11 and fitted these data with eq 3 as indicated by the solid line in the figure. The resultant values of the parameters were $f = 2.91$ cm^{-1}, $g = 4.11$ cm^{-1}, and $h = 1.36$ cm^{-1}. The dashed line in the same figure represents the contribution from the sum of the second and third terms in eq 3.

We then estimated the magnitude of the homogeneous width at $2\rho_c$ for samples with different compositions. An example of the procedure is shown in Figure 11 by the arrows A and B that indicate the data for the particular sample with $x(CO_2) = 0.985$. Namely, the original bandwidth is indicated by the circle marked A, and the magnitude of the homogeneous width is

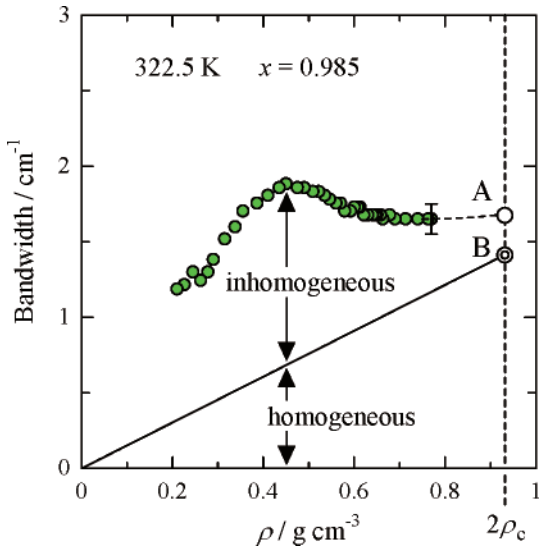

Figure 12. Process of estimation of inhomogeneous broadening. Point B is the magnitude of the homogeneous component estimated in Figure 11. (—) Assumed density dependence of the homogeneous component.

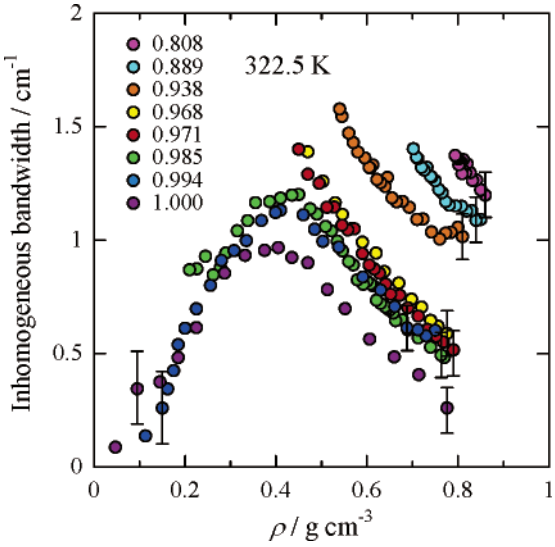

Figure 13. Density dependence of the inhomogeneous bandwidth estimated for samples with different compositions at 322.5 K.

estimated with the dashed line as the double circle marked B. We next transfer into Figure 12 the value of the homogeneous width at $\rho = 2\rho_c$ as marked by the double circle B. The new solid line drawn in Figure 12 is now considered (assumption 4) to represent the density dependence of the homogeneous bandwidth for the sample with $x(CO_2) = 0.985$. The difference between the original plot of the bandwidth and the value of the solid line at every density roughly indicates the magnitude of the inhomogeneous bandwidth we have pursued, although the observed actual band shape is the convolution of the broadenings due to different origins.

In Figure 13, we summarize the results of the density dependence of the inhomogeneous bandwidth estimated as described above for samples of different compositions at 322.5 K. Broad peaks are seen around $\rho = 0.4$ g cm^{-3} for the samples for which phase separation did not take place in the small-density region, while almost monotonous increases of the bandwidth are seen as the density was lowered for the samples for which phase separations were observed. It is noted that the samples with larger contents of benzene show larger inhomogeneous bandwidth if we compare the data at the same density.

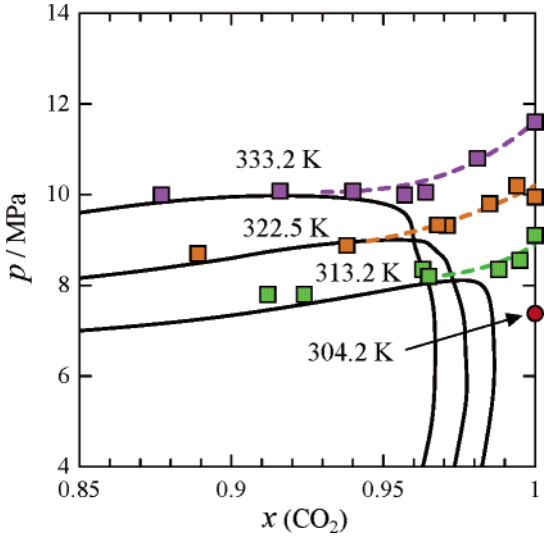

Figure 14. Plot of peak or maximum pressure observed for the inhomogeneous bandwidth of samples with different compositions. Results obtained at three different temperatures are plotted with different colors and form new isothermal curves (---) that approach asymptotically the phase-separation curves (—) at the same temperature. Critical pressure of neat CO_2 is indicated with a red circle.

This is considered to indicate the increasing contribution of CF in the samples with larger contents of benzene in the composition region studied. Similar results were obtained for the data at 313.2 and 333.2 K.

3.5. Distribution of State Points of Large Structural Fluctuation in the Phase Diagram. We now discuss the results by referring to the phase diagram. First, we plot with orange squares in Figure 14 the pressures where the peak or maximum of inhomogeneous bandwidth was observed at 322.5 K for samples with different compositions (see the results shown in Figure 13). We also plot in Figure 14 the corresponding results at 313.2 and 333.2 K with squares of different colors. Note that the composition referred to in this figure is the actual composition of each sample at the state point of the peak or maximum of the inhomogeneous bandwidth. Three solid curves represent the phase-separation curves at the three temperatures. The red circle on the right-hand end of the figure represents the critical pressure of neat CO_2.

In Figure 14, each group of data at three temperatures apparently makes an isothermal line and asymptotically approaches the phase-separation curve at the same temperature. Large CF is expected to occur near the peaks of these phase-separation curves. The data points on the right-hand end of the new isothermal lines represent the pressures where the peak of DF was observed for neat CO_2 at each temperature. These points in fact correspond to the ridge of DF of neat CO_2 reported in our previous paper.[8] Therefore, the new isothermal lines in Figure 14 are considered to connect the point of large CF and the point of large DF at each temperature.

We further examined the evolution of the inhomogeneous bandwidth along the new isothermal lines in Figure 14. The peak or maximum values of the inhomogeneous bandwidth on these lines are plotted in Figure 15 for samples of different compositions at three temperatures. The results show a weak maximum on each isothermal line in Figure 14, the composition of the maximum being almost the same as that of the critical solution point at each temperature. The bandwidths at the right-hand end of these diagrams arise from DF in neat CO_2, while the bandwidth around the composition of the peak in Figure 15 is considered to be dominated by CF. It is noted that the

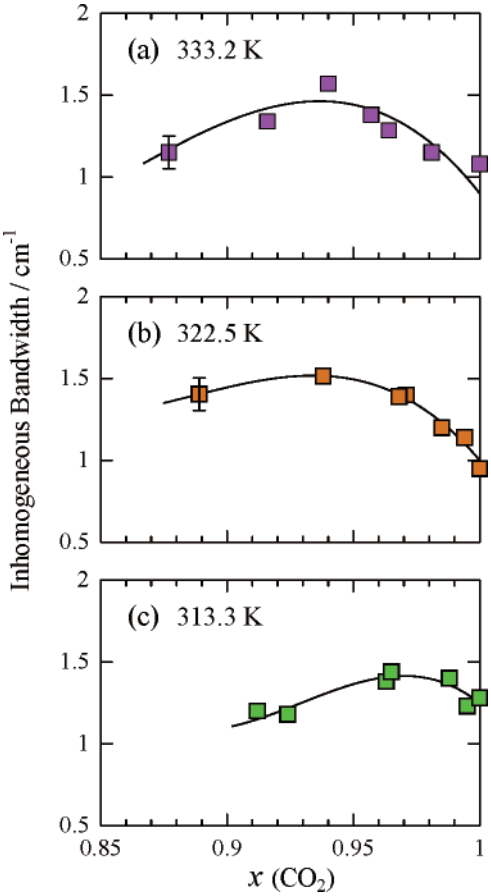

Figure 15. Evolution of inhomogeneous bandwidth on the isothermal lines drawn in Figure 14. The solid lines are the guides to the eye.

inhomogeneous bandwidth at the right-hand end of these figures (representing DF in neat CO_2) decreases as the temperature is raised in this temperature region, because the state point goes away from the critical point of CO_2. On the other hand, the peak values of the inhomogeneous bandwidth on new isothermal lines in Figure 14 are almost the same (compare the peak values of curves a, b, and c in Figure 15). This implies that the magnitude of CF around the critical solution points at these temperatures is not affected strongly by DF of the solvent CO_2.

If one made Raman measurements similar to those described so far at a large number of temperatures, the isothermal lines obtained as in Figure 14 would compose a plane in the TPC three-dimensional phase diagram. This plane may include the ridge of DF of neat CO_2[8] and the line made of critical solution points of the benzene/CO_2 system at every temperature. The situation is schematically depicted in Figure 16 in which the new isothermal lines in Figure 14 are indicated by the solid lines of the same colors (although they are very short). DF may be dominant at the CO_2 end of the plane made of these isothermal lines, while CF may be dominant on the side of the critical solution points. It should be noted that the magnitude of DF in supercritical CO_2 decreases steeply as the state point deviates away from the critical point. Therefore the existence of the above plane may be vague at points far from the critical point of CO_2.

3.6. Solute−Solvent Interaction in Supercritical Binary Systems. Solute molecules may receive solvation if they make attractive interactions with solvent molecules. This is a possible mechanism that brings about additional CF in addition to the general statistical origin. Shulgin and Ruckenstein[26] studied CF of CO_2 in binary solutions by statistical calculations. They

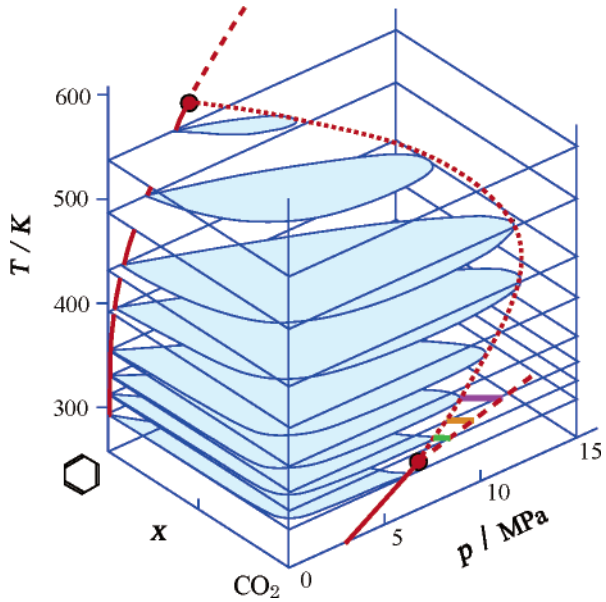

Figure 16. Region of large SF in the TCP three-dimensional space. The new isothermal lines in Figure 14 are drawn with the same colors and seem to compose a sheet in the vicinity of which SF is large. The phase-separation curves of benzene/CO_2 binary systems at different temperatures are drawn on the isothermal planes of corresponding temperatures (compare with those drawn in Figure 1). The red circles and solid red curves represent the critical points and liquid−vapor equilibrium curves of neat benzene and neat CO_2, respectively. The long red dotted curve connects the critical solution points at every temperature.

showed that CF of CO_2 was conspicuously enhanced when they added a small amount of naphthalene to CO_2, while it was not changed from the value of ideal solution when they added ethane. They considered that the phenomenon in the naphthalene case was related to the negative partial molar volume of naphthalene in the vicinity of the CO_2 critical point and is common to many kinds of solutes. On the other hand, the phenomenon observed for ethane was attributed to the similarity between CO_2 and ethane as to the intermolecular force.

The vibrational behavior of solute molecules in the frequency and relaxation time reflects the solute−solvent interaction. For example, Urdahl et al.[27] observed the unusual density dependencies of these quantities of $W(CO)_6$ in supercritical fluids and elucidated the effect of the local density enhancement. On the other hand, Pan et al.[28] reported that neither the Raman wavenumber nor the bandwidth of the vibration of cyclohexane-d_{11} in supercritical CO_2 showed any clear evidence for a local density enhancement. The molecular dynamics simulation by Frankland and Maroncelli[29] elucidated the competition between attractive and repulsive interactions between the solute and solvent molecules and showed that the local density enhancement was small in the same system.

In our present work, we examined the density dependences of the Raman wavenumber and bandwidth of a benzene vibration in CO_2. As described in section 3.2, the studied benzene vibration showed only weak density dependence in the CO_2 solution. One of the reasons for this result may be the fact that the studied benzene vibration is totally symmetric and hardly affected by the electronic polarization of surrounding molecules. Then, the density dependence of the wavenumber, and thus the bandwidth under the density fluctuation also, are considered to have showed weak density dependence.

It should be pointed out that the peak of the phase-separation curve shifts to the CO_2 side (small-concentration side of benzene) as the temperature is lowered (see Figures 1 and 16). Similar behavior is seen in Figure 15 for the inhomogeneous bandwidth. These facts suggest the growth of a specific intermolecular interaction between benzene and CO_2 molecules at lower temperatures, and thus a deviation from ideal solution.

TABLE 1: Values of the Critical Temperature T_c, Critical Pressure p_c, and Acentric Factor ω Adopted in the Calculations

compound	benzene	CO_2
T_c,[a] K	562.05	304.13
p_c,[a] MPa	4.895	7.375
ω	0.212[b]	0.224[c]

[a] Reference 32. [b] Reference 34. [c] Reference 33.

Wada et al.[30] studied IR-absorption intensity of substituted benzene compounds in supercritical CO_2 as a function of density. They observed local enhancement of density around benzene molecules, but its magnitude was small compared with other solute compounds. Otomo and Koda[31] studied ultraviolet spectral shifts of benzene, naphthalene, and chlorobenzene in supercritical CO_2, and showed that the interaction between benzene and CO_2 molecules is small. The results of our studies agree with these results in many respects. However, we consider that the studies of supercritical binary fluids with a strong consciousness of the thermodynamic state in the phase diagram present a new aspect of the solute−solvent interaction in supercritical solutions.

4. Conclusion

We studied the pressure dependence of Raman spectra of benzene/CO_2 binary systems by systematically changing the composition at three temperatures. In these studies, we paid attention to the sample state in the TPC three-dimensional phase diagram. We analyzed the bandwidth of one band of the Fermi dyad of CO_2 and estimated the inhomogeneous component of the width under several assumptions. We found that the region of large inhomogeneity of the sample is spread in the three-dimensional diagram as a sheet that connects the extension curve of the gas−liquid equilibrium curve of neat CO_2 (the ridge of DF) and the curve that connects critical solution points of the binary system on the isothermal plane in the phase diagram. It is considered that the inhomogeneity in the samples is dominated by DF of CO_2 on the side of the above extension curve, while it is dominated by CF on the side of the critical solution points. From the structure of the TPC three-dimensional phase diagram of the benzene/CO_2 binary system and the shift of the peak composition of the inhomogeneous bandwidth, specific intermolecular interaction between benzene and CO_2 molecules was suggested to grow at low temperatures.

Appendix

The parameters a_{mix} and b_{mix} in eq 1 in section 3.4 are defined as follows:

$$a_{mix} = \sum_i \sum_j x_i x_j a_{ij} \quad (4)$$

$$b_{mix} = \sum_i x_i b_i \quad (5)$$

where a_{ij} is related to the parameters a_i and a_j for neat components by

$$a_{ij} = \sqrt{a_i a_j}(1 - \delta_{ij}) \quad (6)$$

a_i was assumed to have a value[23]

$$a_i = \frac{0.45724R^2T_i^2}{p_i}[1 + \kappa_i\{1 - \sqrt{T/T_i}\}]^2 \quad (7)$$

where p_i and T_i are respectively the critical pressure and critical temperature of the ith component, and κ_i is a function of the acentric factor ω_i of the ith component as

$$\kappa_i = 0.37464 + 1.54226\omega_i - 0.26992\omega_i^2 \quad (8)$$

The interaction parameter δ_{ij} in eq 6 includes temperature-dependent parameters K_{ij} and K_{ji} as expressed by

$$\delta_{ij} = K_{ij} - (K_{ij} - K_{ji})x_i \quad (9)$$

We adopted the empirical values of K_{ij} and K_{ji} listed in ref 17 for benzene/CO_2 systems. For the temperatures for which values of K_{ij} are not available, we estimated those by interpolation of the data in ref 17.

The parameter b_i in eq 5 was assumed to have the value[23]

$$b_i = \frac{0.07780RT_i}{p_i} \quad (10)$$

The values of p_i, T_i, and ω_i of CO_2 and benzene adopted in the calculations are summarized in Table 1.

Note Added after ASAP Publication. This article was released ASAP on February 6, 2007. Equation 3 has been revised. The corrected version was posted on February 9, 2007.

References and Notes

(1) Savage, P. E.; Gopalan, S.; Mizan, T. I.; Martino, C. J.; Brock, E. E. *AIChE J.* **1995**, *41*, 1723.
(2) Ekert, C. A.; Knutson, B. L.; Debenedetti, P. G. *Nature* **1996**, *383*, 313.
(3) Kajimoto, O. *Chem. Rev.* **1999**, *99*, 355.
(4) Tucker, S. C. *Chem. Rev.* **1999**, *99*, 391.
(5) Stanley, H. E. *Introduction to phase transition and critical phenomena*; Oxford University Press: New York, 1971.
(6) Morita, T.; Nishikawa, K.; Takematsu, M.; Iida, H.; Furutaka, S. *J. Phys. Chem. B* **1997**, *101*, 7158.
(7) Nishikawa, K.; Morita, T. *J. Supercrit. Fluids* **1998**, *13*, 143.
(8) Nakayama, H.; Saitow, K.; Sakashita, M.; Ishii, K.; Nishikawa, K. *Chem. Phys. Lett.* **2000**, *320*, 323.
(9) Kato, T.; Nakanishi, T.; Fujiyama, T. *Bull. Chem. Soc. Jpn.* **1980**, *53*, 2173.
(10) Scheerboon, M. I. M.; Schouten, J. A. *Phys. Rev. E.* **1995**, *51*, R2724.
(11) Debenedetti, P. G.; Mohamed, R. S. *J. Chem. Phys.* **1989**, *90*, 4528.
(12) Furutaka, S.; Kondo, H.; Ikawa, S. *Bull. Chem. Soc. Jpn.* **2001**, *74*, 1755.
(13) Jin, Y.; Ikawa, S. *J. Chem. Phys.* **2004**, *121*, 2694.
(14) Bamberger, A.; Maurer, G. *J. Supercrit. Fluids* **1994**, *7*, 115.
(15) Peters, J.; C.; Gauter, K. *Chem. Rev.* **1999**, *99*, 419.
(16) Kay, W. B.; Kregkewski, A. *Fluid Phase Equilib.* **1983**, *11*, 251.
(17) Bendale, P. G.; Enick, R. M. *Fluid Phase Equilib.* **1994**, *94*, 227.
(18) Van Konynenburg, P. H.; Scott, R. L. *Philos. Trans. R. Soc. London, A* **1980**, *298*, 495.
(19) Saitow, K.; Nakayama, H.; Ishii, K.; Nishikawa, K. *J. Phys. Chem. A* **2004**, *108*, 5770.
(20) Fujiyama, T.; Kakimoto, M.; Suzuki, T. *Bull. Chem. Soc. Jpn.* **1976**, *48*, 606.
(21) Garrabos, Y.; Tufeu, R.; Le Neindre, B; Zalczer, G.; Beysens, D. *J. Chem. Phys.* **1980**, *72*, 4637.
(22) Tanabe, K.; Hiraishi, J. *Spectrochim. Acta* **1980**, *36A*, 341.
(23) Peng, D. Y.; Robinson, D. B. *Ind. Eng. Chem. Fundam.* **1976**, *15*, 59.
(24) Doge, G.; Yarwood, J. *Spectroscopy and Relaxation of Molecular Liquids*; Steel, D., Yarwood, J., Eds.; Elsevier, New York, 1991; p 274.
(25) Arai, A. A.; Morita, T.; Nishikawa, K. *Chem. Phys.* **2005**, *310*, 123.
(26) Shulgin, I.; Ruckenstein, E. *J. Mol. Liq.* **2002**, *95*, 205.
(27) Urdahl, R. S.; Myers, D. J.; Rector, K. D.; Davis, P. H.; Cherayil, B. J.; Fayer, M. D. *J. Chem. Phys.* **1997**, *107*, 3747.
(28) Pan, X.; McDonald, J. C.; MacPhail, R. A. *J. Chem. Phys.* **1999**, *110*, 1677.
(29) Frankland, S. J. V.; Maroncelli, M. *J. Chem. Phys.* **1999**, *110*, 1687.
(30) Wada, N.; Saito, M.; Kitada, D.; Smith, R. L., Jr.; Inomata, H.; Arai, K.; Saito, S. *J. Phys. Chem. B* **1997**, *101*, 10918.
(31) Otomo, J.; Koda, S. *Chem. Phys.* **1999**, *242*, 241.
(32) Lide, D. R. *CRC Handbook of Chemistry and Physics*, 83rd ed.; CRC Press: Boca Raton, FL, 2002.
(33) Corazza, M. L.; Cardozo-Filho, L.; Antunes, O. A. C.; Dariva, C. *Ind. Eng. Chem. Res.* **2003**, *42*, 3150.
(34) Rolemberg, M. P.; Krähenbühl, M. A. *J. Chem. Eng. Data* **2001**, *46*, 256.